HHS Public Access

Author manuscript

Mol Psychiatry. Author manuscript; available in PMC 2026 February 02.

Published in final edited form as:

Mol Psychiatry. 2025 September ; 30(9): 4320–4333. doi:10.1038/s41380-025-03014-z.

A single-cell genomic atlas for the effects of chronic ethanol exposure in the mouse dorsal striatum

Erin Wildermuth[1,2], **Michael S. Patton**[3,4], **Marcia Cortes-Gutierrez**[1], **Zeal Jinwala**[5,6], **Benjamin H. Grissom**[1,7], **Rianne R. Campbell**[8], **Henry R. Kranzler**[5,6], **Mary Kay Lobo**[8,9], **Seth A. Ament**[1,9,10,✉], **Brian N. Mathur**[4,9,✉]

[1]Institute for Genome Sciences, University of Maryland School of Medicine, Baltimore, MD, USA.

[2]Medical Scientist Training Program, University of Maryland School of Medicine, Baltimore, MD, USA.

[3]Program in Neuroscience, University of Maryland School of Medicine, Baltimore, MD, USA.

[4]Department of Pharmacology and Physiology, University of Maryland School of Medicine, Baltimore, MD, USA.

[5]Center for Studies of Addiction, Department of Psychiatry, University of Pennsylvania Perelman School of Medicine, Philadelphia, PA, USA.

[6]Mental Illness Research, Education and Clinical Center, Crescenz VAMC, Philadelphia, PA, USA.

[7]Program in Molecular Medicine, University of Maryland School of Medicine, Baltimore, MD, USA.

[8]Department of Neurobiology, University of Maryland School of Medicine, Baltimore, MD, USA.

[9]Kahlert Institute for Addiction Medicine, University of Maryland School of Medicine, Baltimore, MD, USA.

[10]Maryland Psychiatric Research Center, Department of Psychiatry, University of Maryland School of Medicine, Baltimore, MD, USA.

Abstract

Alcohol use disorder (AUD) is characterized by compulsive drinking, which is thought to be mediated by effects of chronic intermittent ethanol exposure on the dorsal striatum, the input nucleus of the basal ganglia. Despite significant efforts to understand the impact of ethanol on the

✉**Correspondence** and requests for materials should be addressed to Seth A. Ament or Brian N. Mathur. sament@som.umaryland.edu; bmathur@som.umaryland.edu.

AUTHOR CONTRIBUTIONS

BNM and SAA conceptualized the study. MSP, MC-G, and RRC performed experiments. EW, ZJ, BHG, and SAA performed formal analyses of the data. HRK, MKL, SAA, and BNM supervised the study and acquired funding. EW, SAA, and BNM wrote the original draft. All authors reviewed and edited the manuscript.

ETHICS APPROVAL AND CONSENT TO PARTICIPATE

Animal studies were performed in accordance with NIH guidelines and were approved by the Institutional Animal Care and Use Committee of the University of Maryland Baltimore (Protocol # 0522009). The central Veterans Affairs (VA) institutional review board (IRB) approved the Million Veteran Program study. All relevant ethical regulations for work with human subjects were followed in the conduct of the study and informed consent was obtained from all participants.

dorsal striatum, the rich diversity of striatal cell types and multitude of ethanol targets expressed by them necessitates an unbiased, discovery-based approach. In this study, we used single-nuclei RNA-sequencing (snRNA-seq; n = 86,715 cells) to examine the impact of chronic intermittent ethanol exposure on the dorsal striatum in C57BL/6 male and female mice. We detected 462 differentially expressed genes at FDR < 0.05, the majority of which were mapped to spiny projection neurons (SPNs), the most prominent cell type in the striatum. Gene co-expression network analysis and functional annotation of differentially expressed genes revealed down-regulation of postsynaptic intracellular signaling cascades in SPNs. Inflammation-related genes were down-regulated across many neuronal and non-neuronal cell types. Gene set enrichment analyses also pointed to altered states of rare cell types, including the induction of angiogenesis-related genes in vascular cells. A gene module down-regulated specifically in canonical SPNs was enriched for calcium-signaling genes and components of glutamatergic synapses, as well as for genes associated with genetic risk for AUD. Genetic perturbations of six of this module's hub genes – *Foxp1*, *Bcl11b*, *Pde10a*, *Rarb, Rgs9*, and *Itgr1* – had causal effects on its expression in the mouse striatum and/or on the broader set of differentially expressed genes in alcohol-exposed mice. These data provide important clues as to the impact of ethanol on striatal biology and provide a key resource for future investigation.

INTRODUCTION

Alcohol Use Disorder (AUD) is characterized by compulsive intake of alcohol, often following a chronic, relapsing pattern over many years. AUD affects >5% of the global population and is associated with enormous medical and economic consequences, including ~140,000 annual deaths from alcohol-related causes in the United States alone [1]. Only three medications are approved for AUD treatment in the United States, and they each provide limited efficacy [2]. A more complete understanding of alcohol's effects in the brain would lead to the identification of targets for novel, potentially more effective therapies.

The dorsal striatum is a key structure dysregulated in humans with AUD, as well as in animal models of chronic alcohol intake [3]. The dorsal striatum is the input nucleus of the basal ganglia, receiving excitatory glutamatergic inputs from the thalamus and cortex, as well as modulatory dopaminergic inputs from the substantia nigra pars compacta [4]. Outputs from the striatum are funneled through two distinct pathways -- the "direct" striatonigral pathway and "indirect" striatopallidal pathway -- which have distinct, often opposing effects on the activity of downstream circuit elements in the pallidum, thalamus, and other regions [5–7]. GABAergic spiny projection neurons (SPNs) comprise ~95% of striatal neurons. Molecularly distinct SPN subtypes marked by expression of D_1 vs. D_2 dopamine receptors form the direct and indirect pathways, respectively. SPNs are modulated by GABAergic and cholinergic interneurons and supported by numerous subtypes of glia and other non-neuronal cells.

Alcohol actions on the dorsal striatum are thought to foster the expression of actions related to alcohol seeking and its compulsive consumption [8]. Ethanol is a highly promiscuous ligand, and complex, cell-type specific physiological sequelae in dorsal striatum arise secondary to alcohol exposure [9]. Major neuronal physiological effects of ethanol influence

glutamatergic synapses, GABAergic synapses, and morphological and intrinsic excitability [10–18]. Several modulatory transmitter systems in the dorsal striatum are also affected by alcohol, including brain-derived neurotrophic factor (BDNF) signaling, acetylcholine, endocannabinoids, opioids, and dopamine [19–23]. Given this complexity, there is a need for cellular-resolution studies to understand the nature of these diverse effects and the cellular sources of the expression changes driving them.

Single-nuclei RNA sequencing (snRNA-seq) has emerged as a powerful strategy to describe the cell type-specific molecular adaptations associated with exposure to addictive substances [24, 25], building on prior observations of gene expression differences from mRNA sequencing of bulk tissue [26–28]. To date, only a few snRNA-seq studies have described changes in AUD or AUD-related animal models, including studies of the prefrontal cortex, amygdala, and nucleus accumbens [9, 29–32]. However, to our knowledge, there have been no published reports describing snRNA-seq of the dorsal striatum from an animal model of chronic ethanol exposure. Here, using snRNA-seq, we describe cell type-specific transcriptional changes in the dorsal striatum of mice exposed to chronic intermittent ethanol (CIE).

METHODS

Animals

Male and female C57BL/6 J mice (4–6 months) were housed with littermates (2–5 per cage) under a normal 12 h light/dark cycle (lights on at 0900 h, off at 2100 h) with ad libitum access to food (LabDiet 5010) and water.

Chronic intermittent ethanol (CIE)

Mice were placed in Plexiglass inhalation chambers (60 × 36 × 60 cm) and exposed to ethanol vapor or air 16 h/day, 4 days a week for a total of 5 weeks. Ethanol was volatilized by passing air through a tube submerged in 95% ethanol. After 4 days in the inhalation chambers, mice underwent a 72 h forced abstinence period from ethanol. Control vapor chambers delivered only air without ethanol vapor. Vapor chamber ethanol concentrations were monitored daily, and air flow was adjusted to produce ethanol concentrations within 1.8–2.0% ethanol content measured by a digital alcohol breath tester (FFtopu). These conditions produce stable blood ethanol concentrations in C57BL/6J mice ranging from 150–200 mg/dl [33]. The alcohol dehydrogenase inhibitor pyrazole (1 mmol/kg, i.p.) was injected daily in both control and ethanol treated mice during weeks 4–5 to stabilize blood ethanol concentrations, as alcohol dehydrogenase function is upregulated following 3-weeks of CIE treatment [33].

Tissue collection

Brains were collected in the morning (~10 AM), exactly 3 days (72 h) after the final exposure to vaporized ethanol (or air) following previously established methods to ensure that ethanol was fully metabolized [17]. Mice were sacrificed by rapid decapitation and brains were immediately removed for tissue collection. The dorsal striatum (AP: +1.3 – 0.3 from bregma) was dissected from a 1 mm coronal section cut from a mouse brain mold [8].

Left and right hemispheres were pooled and flash frozen in crushed dry ice. The tissue was stored at −80 °C until further processing. Our primary, discovery dataset included sixteen C57BL/B6 mice equally divided between male and female. Each of our replication datasets included 8 mice equally divided between male and female.

Isolation of cellular nuclei and single-nuclei RNA sequencing (snRNA-seq)

Distinct nuclei isolation protocols were used in the discovery dataset and in each of two batches that comprise the replication dataset. For the discovery dataset, cellular nuclei were isolated from frozen dorsal striatal tissue following a 10× Genomics Demonstrated Protocol (CG000124.RevE) with modifications. Tissue was homogenized in 150 μL lysis buffer for nuclei extraction. To remove cellular debris and large clumps, an Iodixanol density gradient was used. An 8.5% iodixanol (OptiPrep™ Density Gradient, Millipore) buffer serves as a cushion to remove membranes at 1000 × g/10 min at 4 °C. Clean nuclei were collected in the pellet. Propidium iodide was used to determine the nuclei concentration using a MoxiGoII bench cytometer (Orflo), and nuclei aggregation and clumping were evaluated under 60× magnification in a fluorescent microscope and brightfield. Nuclei from one male mouse and one female mouse of the same ethanol treatment group were pooled. Approximately 20,000 nuclei per pooled sample were loaded into a Chromium X microfluidics controller (10× Genomics, Pleasanton, CA). 10× Genomics NextGEM 3′ GEX sequencing libraries were prepared from each sample following manufacturer's instructions and sequenced to a depth of ~50,000 raw reads per cell on a NovaSeq6000 sequencer (Illumina).

For both batches in the replication dataset, nuclei were isolated from frozen brain tissue following a published protocol with our slight modifications [34, 35]. Briefly, frozen brain tissue was disaggregated by pipetting up and down in chilled extraction buffer consisting of Poly(1-vinylpyrrolidone-co-vinyl acetate) (Sigma #190845), 0.1% TritonX-100, and 1% bovine serum albumen (BSA) in dissociation buffer (DB; 82 mM Na2SO4, 30 mM K2SO4, 10 mM Glucose, 2.5 mM MgCl2,10 mM Hepes pH7.4, and RNase inhibitor [Protector, Roche]). Pellets containing nuclei were resuspended in DB and filtered with 70 and 40 μm strainers. To separate nuclei from debris, the nuclei suspension was mixed in a 25% (final) iodixanol layer over a 27% iodixanol cushion, followed by centrifugation (13000 g × 20 min, 4 °C), then nuclei were washed twice in DB. In the second replication dataset, nuclei were labeled with sample-specific oligonucleotide tag using CellPlex reagents, following a validated protocol (CG000391). Finally, nuclei were counted using a MoxiGoII (Orflo) cytometer, and the concentration was adjusted to 365 nuclei/ul in phosphate buffered saline with 2% BSA. 17,000 nuclei were loaded in each well of a Chromium Controller (10× Genomics). Nuclei from four male and four female mice were pooled in each sample. Sequencing libraries were prepared using NextGEM 3′ Gene Expression reagents (10× Genomics), following manufacturer's instructions and sequenced on HiSeq4000 (Replication Batch 1) and NovaSeq6000 (Replication Batch 2) sequencers.

snRNA-seq data analysis

The discovery and replication datasets were analyzed separately because we found that this approach led to the most precise cell clustering and because the distinct pooling

strategies necessitated separate downstream analyses of differential gene expression. In each dataset, genome alignment (mm 10), cell calling, and read counting were performed with cellranger count (v7.1.0), Doublets were detected and removed via scDblFinder [36]. Cells then underwent standard quality control and gene expression data processing with Seurat [37]. Cells with a minimum of 500 reads, no more than 5000 reads, and <20% of reads from mitochondrial genes were selected for initial inclusion. Integration was accomplished using Seurat's SCTransform() pipeline, using 3000 features as integration anchors. Cell clusters were obtained via Louvain clustering (resolution = 0.5) of a shared nearest neighbors graph derived from the first 30 principal components of the integrated data. We applied Uniform Manifold Approximation and Projection (UMAP) to visualize the clusters on two-dimensional plots. We assigned clusters to major cell types based on established markers. Neuronal and non-neuronal subtypes were then separated, and the same dimension reduction and clustering procedures were completed within each grouping to refine subtype clustering and identification, then recombined these results to produce the final cell annotation. At each step, cell clusters with mixed markers were dropped, as these most likely represent doublets. The primary clustering analysis revealed heterogeneity within the eSPN population. To further evaluate eSPN subtypes, we integrated the combined eSPNs from the discovery and replication datasets using Harmony, followed by Louvain clustering with Seurat (30 Harmony dimensions, resolution = 0.3) [38].

As noted above, library preparation and sequencing were performed using pooled cells from male and female mice. We demultiplexed the male vs. female cells within each pooled sample based on the universally expressed female-specific marker gene *Xist*. First, we performed zero-preserving imputation of read counts with ALRA [39] to reduce dropouts. Then, cells with normalized *Xist* expression values greater than the median were assigned as female, and cells with expression values below the median were assigned as male. In most cell types, we were able to validate that Y chromosome genes were expressed much more highly in cells assigned as male, though the low expression of Y chromosome genes made this difficult to evaluate in rare cell types. We note that as with all multiplexing strategies a small proportion of cells are ambiguous, and in this case cells with low read counts tend to be called as male by our algorithm. This was accounted for by performing batch effects corrections on pseudobulk counts prior to performing downstream analysis and by including an effect of sex in the differential gene expression analysis (see below), and we believe it has minimal impact on our estimates for the effects of ethanol exposure. However, estimates for the main effects of sex are not presented, as these may be unreliable due to the bias toward lower read counts in cells assigned as male.

Effects of ethanol exposure on differential gene expression in each cell type were calculated using negative-binomial generalized linear models implemented with edgeR [40], based on the pseudobulk read counts pooled from all the cells of each cell type in each mouse. Pseudobulk analysis avoids anticonservative p-values that have been encountered in models that treat individual cells as the unit of replication [41]. The first step of our analysis using pseudobulk counts was to assess the proportion of variance explained by CIE exposure, sex differences, batch differences, and residuals, using the variancePartition R package. Non-neglible batch differences were found in the discovery dataset. Therefore, we used ComBat-seq [42] (implemented in the sva R package) to adjust for batch effects across eight sample

processing batches, corresponding to a male batch and female batch for each day on which samples were processed. We evaluated with variancePartition that this approach reduced batch effects and boosted the proportion of variance explained by CIE exposure. Samples for each of the two replication datasets were processed separately, so no batch correction was performed. We filtered out genes with very low expression in the batch-corrected, pseudobulk read counts (minimum total reads = 15, including a minimum of 3 counts in one sample). We then fit the counts to a quasi-likelihood generalized linear model and estimated the effects of ethanol using the glmQLFit() and glmQLFTest() functions from the edgeR R package, treating sex as a covariate. In the discovery dataset, we also analyzed sex-specific effects of CIE using *post hoc* contrasts. Differential gene expression analysis was performed separately in each dataset and cell type. We then performed meta-analyses using the sum of weighted z-scores, where the weights were proportional to the number of cells of each cell type within each dataset. A "replication meta-analysis" was performed to combine the two replication datasets to obtain the replication results. A meta-analysis combining all of the discovery and replication datasets was used to produce the *p*-values used in downstream analyses. If a cell type was represented by fewer than 100 cells in a dataset, that dataset was excluded from the meta-analysis. A significance threshold was set globally across all cell types at a False Discovery Rate (FDR) < 5%. P-values from the meta-analysis were used in downstream analysis. For analyses that required fold change estimates, we used the fold changes from the discovery dataset. For comparisons of differentially expressed genes across cell types, we further filtered out genes that had 10-fold higher expression in another cell type, based on pseudobulk counts per million. This filter was intended to reduce false-positive correlations between cell types due to ambient RNA.

Gene set enrichment analysis

Gene sets from Gene Ontology, SynGO, and KEGG were downloaded from the Enrichr database (https://maayanlab.cloud/Enrichr/#libraries) on December 6, 2023. For gene set enrichment analyses of cell type differentially expressed genes, we applied the geneSetTest() function from the limma R package to test enrichments among up- and down-regulated genes (separately) from each cell type [43]. For gene set enrichment analysis of gene co-expression modules we tested for enrichment using Fisher's exact tests. For visualization purposes, we calculated Cohen's kappa to compare gene sets and plotted only those terms for which no term with k > 0.5 had a stronger p-value.

Gene co-expression networks

Gene co-expression modules in spiny projection neurons were identified via an imputation and clustering procedure, with slight modifications from our published work [44]. We started from the read counts in 8535 dSPNs, iSPNs, and eSPNs from our snRNA-seq of four mice processed on the same day (discovery dataset in Table S1; one per sex per group). Selecting cells from a single processing batch was intended to reduce technical variation among the samples. We removed genes with read counts in fewer than 3% of these cells. Read counts were imputed with ALRA to improve correlation structure in the data, followed by normalization as counts per million, log-transformation, zero-centering, and scaling to unit variance. Next, we performed k-means clustering using the kmeans() function in R with k = 50, Lloyd's algorithm, 10 starts, and up to 10,000 iterations. Finally, the clustering

results were refined by merging clusters whose centroids were strongly correlated (Pearson's $r > 0.7$) and by removing genes that were weakly correlated with the centroid of the module to which they had been assigned ($r < 0.3$). We tested for enrichment of modules among differentially expressed genes using Fisher's exact tests, using a lenient differential expression threshold ($P < 0.01$) to improve statistical power. Hub genes were identified by ranking each module's genes by their correlation with the module centroid (kCentroid). All of these analyses of network structure were performed in the training data to avoid technical correlations associated with batch. We evaluated network preservation statistics to validate that gene co-expression modules identified in a subset of the dataset are preserved in the remainder of the data. We scored the expression of modules across our entire snRNA-seq dataset using the addModuleScore() function in Seurat. Using these module centroid scores, we tested that each module's hub genes are preserved across batches; i.e., whether the same genes are the most strongly correlated with the module's centroid in each batch. In addition, we tested that the strength of the correlations between each module's centroid and its hub genes were similar across batches. We also used module centroids applied to the entire dataset to visualize the expression of modules across cell types and groups.

Spatial transcriptomics

Spatial transcriptomics experiments were performed with the CosMx Spatial Molecular Imager (NanoString, Seattle, WA), using the 1000-gene Mouse Neuroscience Panel to validate the cell type-specificity of differentially expressed genes and modules. The forebrain of an 8-week old, male mouse was formalin-fixed, coronally cut into 5 mm slices and placed in cassettes for paraffin-embedding. These formalin-fixed paraffin embedded (FFPE) blocks were sectioned on the microtome, where 5 μm FFPE scrolls were cut, then transferred to a RNAse-free molecular grade water bath. Floating sections were placed on a microscope slide, processed, and imaged following manufacturer's instructions. Initial image processing, including cell segmentation and read counting, were performed with AtoMx (NanoString). Cell clustering was performed with Seurat using 49 principal components -- excluding the first principal component, which was strongly correlated with the number of UMIs – and Louvain clustering at a manually-determined resolution of 1.0. Clusters were annotated to known cell types by comparison to cell type markers from snRNA-seq. Of 131,548 cells called by AtoMx, 11,663 were excluded as likely doublets in clusters with mixed markers, and downstream analyses were performed with the remaining 119,885 high-quality cells. Spiny projection neurons were sub-clustered with Seurat (5 principal components, resolution = 0.5) to evaluate their spatial distribution within the striatum. Cell type-specificity of DEGs (from snRNA-seq) was examined by plotting their expression on UMAPs, violin plots, and spatial expression plots. Cell type-specificity for modules by scoring their expression in each cell using the AddModuleScore() function from Seurat.

Integration with results from genome-wide association studies (GWAS) of alcohol use disorder

We used GWAS summary statistics from Kember et al. to test whether differentially expressed genes and gene networks in CIE-exposed mice were associated with genetic risk for AUD [45]. We performed MAGMA [46] gene property analyses to test whether up-

and down-regulated genes in each striatal cell type were enriched at AUD risk loci. We performed MAGMA gene set analyses to test whether SPN gene co-expression modules were enriched at AUD risk loci.

Analysis of mRNA-seq from the striatum of mice heterozygous for module M43 hub genes

Wang et al. performed mRNA-seq of striatal tissue from six-month-old heterozygous knockout mice and wildtype littermate controls for 52 genes (n = 3 male and n = 3 female mice per genotype) [47]. Details of their study design are contained in the original paper. The genes investigated by Wang et al. were selected based on their expression patterns in the striatum of Huntington's disease knock-in mice. Seven of the genes overlapped Module M43 from our gene co-expression analysis, enabling us to test the hypothesis that each genetic perturbation causally regulates the expression of genes in Module 43. We downloaded the mRNA-seq read counts and sample metadata (GSE149900). We computed differential gene expression in each heterozygous genotype compared to wildtype controls using voom/limma, treating sex as a covariate [48]. We applied multiple metrics to evaluate the relationship between heterozygous knockout (HetKO) conditions and the effects of CIE. We used Fisher's exact tests to evaluate whether the up- and down-regulated genes in each knockout line (FDR < 0.05) were enriched among the genes in M43, as well as among the broader set of differentially expressed genes. We used the moduleEigengenes() function from WGCNA to score M43 activity in each sample. We tested correlations between the log(fold change) responses to HetKO vs. CIE.

RESULTS

A single-cell genomic atlas for the effects of chronic ethanol exposure in the dorsal striatum

Chronic Intermittent Ethanol (CIE) is a widely used paradigm to model the effects of moderate to heavy alcohol consumption [33, 49, 50]. Previous studies have shown that CIE and related paradigms lead to cell type-specific physiological changes in striatal neurons, but the molecular mechanisms remain poorly understood. To gain insight, we performed 10× Genomics single-nuclei RNA sequencing (snRNA-seq) in the dorsal striatum of four-month-old C57BL/6J mice that had undergone five weeks of CIE, compared to age- and sex-matched controls (Fig. 1A, B). We used a two-stage meta-analysis to discover and replicate effects of CIE. In our discovery dataset, we sequenced nuclei from n = 8 CIE-exposed mice and 8 controls (n = 4 male and female mice per group), yielding 70,934 high-quality cells (31,225 CIE, 39,709 controls). In our replication dataset, we performed snRNA-seq of pooled samples from 8 additional CIE-exposed mice and 8 controls, yielding 15,781 high-quality cells. The lower number of cells in the replication dataset is expected due to the pooling strategy. Data quality metrics are shown in Table S1.

Cells in each snRNA-seq dataset were clustered and assigned to 12 cell types based on established cell type markers (Fig. 1C, D; Figs. S1, S2; Tables S2, S3). Neuronal subtypes included direct pathway spiny projection neurons (dSPNs; *Drd1*+), indirect pathway spiny projection neurons (iSPNs; *Drd2*+), atypical spiny projection neurons (termed "eccentric", eSPNs; *Otof*+), cholinergic interneurons (IN-Chat; *Chat*+), parvalbumin

interneurons (IN-PV; *Gad1*+, *Kit*+), and somatostatin interneurons (IN-Sst; *Gad1*+, *Sst* +). Non-neuronal cell types included astrocytes (*Slc1a3*+, *Rorb*+), oligodendrocytes (*Mog*+, *Aspa*+), oligodendrocyte precursor cells (*Pgdfra*+, *Coll11a1*+), mural cells (*tn*+, *Pgdfrb*+), endothelial cells (*Flt1*+, *Slco1a4*+), ependymal cells (*Rsph1*+), and microglia (*Cx3Cr1*+, *C1qc*+). eSPNs are a heterogeneous population represented by two distinct clusters on the UMAP (Fig. 1C). The two major eSPN subtypes, marked by *Cnr1/Otof* and *Grm8/Chst9*, respectively, were present in roughly similar proportions in the discovery and replication datasets (Fig. S3).

We characterized differentially expressed genes (DEGs) in CIE-exposed vs. control animals using a conservative pseudobulk approach. Batch differences were identified in the pseudobulk counts, and removing batch effects with ComBat-seq boosted signal (Fig. S4). In our discovery dataset, we found 497 cell type specific DEGs at a False Discovery Rate (FDR) < 0.05. DEGs were identified in all cell types, yet the vast majority were detected in SPNs, with 176, 92, and 135 DEGs in dSPNs, iSPNs, and eSPNs, respectively, compared to fewer than 30 DEGs in all other cell types (Fig. 2A; Fig. S5; Table S4).

In our replication dataset, we found 460 cell type specific DEGs at FDR < 0.05, and again DEGs were detected primarily in SPNs (Fig. 2A, middle; Tables S5–S7). We note that some genes had unusually large fold changes in the replication dataset, which may relate to inflation of effect sizes in this relatively small dataset or to the effects of pooling. 37 DEGs were reproducible at FDR < 0.05 in both the discovery and replication datasets (more than expected by chance: Fisher's exact test, odds ratio = 33.9, $P = 6.2e{-}50$). In addition, 141 of the 497 DEGs from the discovery dataset replicated at a nominal p-value < 0.05. Notably, most of the highly-reproducible DEGs were down-regulated in both dSPNs and iSPNs, with somewhat stronger p-values but similar fold changes in dSPNs (Fig. 2B). Most of these genes were differentially expressed specifically in SPNs and not in other striatal cell types (Fig. 2C).

We also analyzed the effects of CIE in males and females separately. Since cells from male and female animals were pooled in each sample, this analysis relied on demultiplexing the male and female cells in each sample based on the expression of the female-specific transcript *Xist*. We validated this strategy by confirming that a Y chromosome transcript, *Uty*, was expressed more highly in cells determined to be male than in those determined to be female (Fig. S6). We then analyzed sex-specific effects of CIE using *post hoc* contrasts in edgeR. Sex-specific DEGs (FDR < 0.05) were detected primarily in SPNs (Table S8), consistent with our analyses of the two sexes combined. Interestingly, we detected substantially more DEGs in dSPNs and iSPNs from males than from females (Fig. S7). Comparing the fold changes of DEGs suggested that the effects of CIE were usually in the same direction in both sexes, but the magnitude was often larger in males than females (Figs. S7–S9). By contrast, in eSPNs we detected similar numbers of DEGs in males and females and the fold changes were similar (Fig. S7). Despite these differences in magnitude, we detected very few effects of CIE that were truly sex-specific, and statistical power was generally stronger when the two sexes were combined.

We applied a threshold-free approach, rank-rank hypergeometric overlap (RRHO) [51], to evaluate the reproducibility of differential expression patterns in specific cell types. This analysis revealed significant reproducibility of differential expression ranks (FDR < 0.05) in dSPNs, iSPNs, eSPNs, IN-PV, astrocytes, and OPCs, again with the strongest effects in SPNs (Fig. 2D). We note that three rare cell types – endothelial cells, mural cells, and cholinergic interneurons – were detected too infrequently in the replication dataset (fewer than 100 cells each) to be included in these analyses of reproducibility, though each displayed intriguing effects in the discovery dataset.

We performed a meta-analysis across the discovery and replication datasets (both sexes) to obtain a final list of differentially expressed genes. In the meta-analysis, we detected 462 DEGs at FDR < 0.05, including 248, 82, and 94 DEGs in dSPNs, iSPNs, and eSPNs, respectively, and ten or fewer DEGs in each of the other cell types (Fig. 2A, right; Table S9). We note that artifacts from ambient RNA, doublets, or mis-clustering can cause certain highly-expressed genes with variable expression across cell types to appear as common false positives in snRNA-seq differential expression analysis. One example is *Ptgds* (Fig. 2C). We flagged 76 DEGs that had >10-fold higher expression in another cell type as likely false positives (Table S9) and excluded them from downstream analyses. We also note that our meta-analysis technique does not produce a fold change estimate. Our downstream analyses used p-values from the meta-analysis alongside fold changes from the discovery dataset.

Shared vs. cell type-specific effects of ethanol exposure across striatal cell types

Next, we performed gene set enrichment analyses to characterize the functional categories perturbed in each cell type, and we compared these effects across cell types. We used a threshold-free algorithm, limma's geneSetTest [43], which enabled us to find significant gene sets even for cell types in which few individual DEGs were detected. These analyses revealed both cell type-specific gene sets enriched for up- or down-regulated genes, as well as gene sets that were dysregulated in multiple cell types (Fig. 3; Table S10).

Amongst the more cell type-specific effects, we found that synapse-related gene sets, including components of glutamatergic synapses and genes involved in axon guidance were down-regulated primarily in SPNs: Glutamatergic Synapse (KEGG) in dSPNs, $P = 6.3e{-3}$; in iSPNs, $P = 6.8e{-3}$; Axon guidance (GO:0007411), in dSPNs, $P = 2.5e{-4}$, in iSPNs, $P = 9.2e{-9}$. Down-regulated components of glutamatergic synapses in dSPNs (FDR < 0.05) included the synaptic scaffolding protein *Homer1*, the voltage-gated calcium channel subunit *Cacna1a*, and the glutamate receptor subunits *Grm5, Grik2*, and *Gria4*. In the adult brain, many axon guidance genes help maintain synapses. Down-regulated genes annotated to this pathway included *Reln, Unc5c*, and *Plxna1*, amongst others. These results suggest a specific vulnerability of spiny projection neuron synapses to CIE.

We also found cell type-specific effects of ethanol exposure in endothelial cells, including enrichment of endothelial cell DEGs for genes involved in the regulation of cell population proliferation (GO:0042127, $P = 1.3e{-6}$). Differentially expressed genes in this category (FDR < 0.1) included the Notch effector *Hes1* (down-regulated, unadjusted $P = 2.9e{-5}$), as well as *Tgfb2*, which encodes transforming growth factor-beta 2 (up-regulated, $P = 6.0e{-5}$).

Endothelial cells are the major cell type of blood vessels in the brain, so we speculate that these changes may relate to the effects of ethanol exposure on angiogenesis [52–54].

Several categories of genes were dysregulated across multiple cell types. For instance, at FDR < 0.1, components of ribosomes (KEGG, “Ribosome”) were enriched for differential gene expression in eight cell types. Genes involved in the regulation of transcription by RNA Polymerase II (GO:0006357) were up-regulated in astrocytes, oligodendrocytes, and endothelial cells. Genes involved in mitochondrial ATP synthesis-coupled electron transport were down-regulated in astrocytes, OPCs, and oligodendrocytes but up-regulated in dSPNs. These results suggest complex effects of CIE on the regulation of transcriptional and energy metabolism.

We studied the fold changes of individual DEGs across cell types to gain further insight into these shared vs. cell type-specific effects. First, we calculated the correlations of fold changes across all DEGs. This analysis revealed strongly correlated effects of CIE in dSPNs and iSPNs (Pearson’s r = 0.86, $P = 7.3e–89$; Fig. 4A), and 53 genes were differentially expressed at FDR < 0.05 in both subtypes (Fig. 4B). A biplot revealed that nearly all DEGs had similar effect sizes in both of these SPN subtypes (Fig. 4C). Fold changes in eSPNs were somewhat more modestly correlated with fold changes in dSPNs (r = 0.56) and iSPNs (r = 0.54), and there were only 7 DEGs in common amongst all three SPN subtypes. Biplots confirmed a mix of shared and subtype-specific effects when comparing eSPNs to the canonical SPN subtypes (Fig. 4D, E). We also found more modest, positive correlations in fold changes in other cell types, reflecting the shared functional categories described above. Across all pairs of cell types, the median correlation coefficient among DEG fold changes was r = 0.29 (Fig. 4A).

We generated spatial transcriptomics data with the NanoString CosMx platform to validate the cell type-specificity of DEGs. We assayed the spatial expression patterns of 1000 genes in a coronal section from the mouse forebrain, including many brain cell marker genes and 12 of the top DEGs identified in SPNs (FDR < 0.01). Clustering of 119,885 high-quality cells identified clusters corresponding to 13 neuronal and non-neuronal cell types (Fig. S10; Table S11), including 15,862 SPNs (Fig. S11; Table S12). We confirmed that all 12 of the DEGs included in the CosMx panel were expressed robustly in SPNs, with variable expression in other neuronal and non-neuronal populations (Fig. S12).

Dysregulation of synaptic and neuroinflammatory gene networks in spiny projection neurons

We performed a gene co-expression network analysis to further characterize the effects of ethanol exposure. We analyzed gene-gene correlation structure specifically within SPNs since they had the largest transcriptional responses. k-means clustering of SPN gene expression profiles revealed 45 modules of co-expressed genes (Fig. 5A; Table S13). We confirmed that these modules were reproducible in multiple independent batches of cells within our dataset (Fig. S13). Projection of the modules into our entire snRNA-seq and CosMx spatial transcriptomics datasets revealed varied patterns of specificity to SPNs and other striatal cell types (Figs. S14–S16). We prioritized CIE-related modules by testing each module’s over-representation among differentially expressed genes in CIE vs. control

animals (Fig. 5B; Table S14). This analysis again focused on SPNs, but we also tested for over-representation among DEGs in other cell types to determine whether some effects of CIE may be broader.

Three modules (M29, M43, and M26) were over-represented among genes down-regulated in SPNs (Bonferroni-adjusted *p*-value < 0.01) with little evidence of differential expression in other cell types. M29 displayed similarly strong associations with CIE in the three SPN subtypes (dSPNs, iSPNs, and eSPNs), whereas M43 was primarily associated with DEGs in canonical SPNs (dSPNs and iSPNs) and M26 was most strongly associated with DEGs in eSPNs. The ten most strongly differentially expressed genes in each of these modules are shown in Fig. S17. These modules were enriched for genes with neuron-specific functions (Table S15). M29 was enriched for genes in the transmembrane receptor protein tyrosine kinase signaling pathway (7 genes, OR = 5.5, un-adjusted $P = 5.2e{-4}$), including the BDNF receptor *Ntrk2* (also known as trkB). M43 was enriched for genes in the calcium signaling pathway (11 genes, OR = 11.1, $P = 3.0e{-8}$) and other genes localized to glutamatergic synapses (9 genes, OR = 12.4, $P = 2.1e{-7}$), including components of voltage-gated calcium channels (*Cacnb2*, Cacna2d3), glutamate receptors (*Grid2, Grm5, Gria3*), and the cAMP signaling cascade (e.g., *Pde10a, Pde7b*, *Adcy5, Rgs9*). M26 was enriched for a variety of genes localized to neuron projections (43 genes, OR = 3.1, $P = 2.9e{-9}$), including axon guidance genes (18 genes, OR = 4.1, $P = 3.1e{-6}$; e.g., *Sema6a*). These results support that chronic alcohol exposure leads to SPN-specific down-regulation of numerous synaptic components and related genes.

Module M8 was enriched for down-regulated DEGs in all three SPN subtypes, as well as in nearly all other neuronal and non-neuronal cell types in the striatum. M8 was most strongly enriched for genes involved in cytokine-cytokine signaling interactions (10 genes, OR = 7.4, $P = 5.5e{-6}$), as well as other genes involved in the regulation of inflammatory responses (10 genes, OR = 3.9, $P = 6.4e{-4}$). These results suggest that chronic alcohol exposure leads to neuroinflammation-related transcriptional changes that impact most or all striatal cell types.

Two modules (M24 and M18) were enriched for up-regulated DEGs. M24 was up-regulated primarily in dSPNs, whereas M18 was up-regulated primarily in eSPNs. Both of these modules were comprised of genes with rather diverse functions. Functional enrichments for M24 included sequence-specific DNA binding (27 genes, OR = 2.3, $P = 1.7e{-4}$), but also actin cytoskeleton (19 genes, OR = 2.1, $P = 0.004$) and inorganic ion transmembrane transport (16 genes, OR = 2.2, $P = 0.005$). Functional enrichments for M18 included regulation of cell migration (13 genes, OR = 3.0, $P = 0.001$) and calcium ion binding (10 genes, OR = 3.2, $P = 0.002$). Thus, CIE was associated with diverse transcriptional effects that were relatively subtle and cell type-specific compared to down-regulated processes.

Associations of CIE-related genes with genetic risk for alcohol use disorder and prioritization of drug targets

We evaluated the disease relevance of differential gene expression patterns in CIE-exposed mice via comparisons to genetic studies of human alcohol use disorder (AUD). We analyzed summary statistics from a published genome-wide association study (GWAS) of AUD cases and controls in the Million Veteran Program [45, 55], using MAGMA to test for overlap

of AUD risk genes with cell type-specific DEGs and gene co-expression modules. Twenty-six of the DEGs in CIE-exposed mice had nominally significant GWAS *p*-values < 0.05, including six with a study-wide false discovery rate < 5% (adjusting for multiple testing across 208 DEGs with GWAS results; Fig. S18A; Table S16). We found significant overlap (FDR < 0.1) of AUD risk genes with genes up-regulated in eSPNs (MAGMA: beta = 0.03, $P = 8e{-}4$) and astrocytes (beta = 0.02, $P = 2.8e{-}3$; Table S17), with the strongest shared associations to the sodium/calcium exchanger *SLC8A3* (GWAS: $P = 4.9e{-}3$; snRNA-seq: logFC in eSPNs = 0.82, $P = 7.6e{-}6$) and the transcription factor *NFATC1* (GWAS: $P = 1.3e{-}5$; snRNA-seq: logFC in astrocytes = 0.55, $P = 7.9e{-}3$). In addition, we found a significant overlap of AUD risk genes with genes in module M43 (beta = 0.20, $P = 0.002$; Table S18). Fourteen of the 108 genes in module M43 had nominally significant associations both with AUD risk and CIE differential expression: *INO80E*, *PLCB1*, *PRKCB*, *HS6ST3*, *NEGR1*, *CALN1*, *BCL11B*, *NRG1*, *ROBO2*, *LRRC7*, *PARD3*, *DCC*, *ATXN1*, and *PDE10A*. Thus, a subset of DEGs in CIE-exposed mice may contribute to risk for AUD.

Hub genes of gene co-expression modules are candidate drug targets because their perturbation frequently has causal effects on gene expression and on downstream physiological and behavioral traits. We focused on module M43, owing to the convergent evidence from its dysregulation in CIE-exposed mice and its association with genetic risk for AUD. We tested causal roles for seven M43 hub genes using publicly available mRNA-seq of bulk striatal tissue from six-month-old heterozygous knockout (HetKO) mice [47]. The tested genes included four transcription factors (*Bcl11b, Foxp1, Rarb*, and *Zswim6*), as well as *Pde10a*, a phosphodiesterase, *Rgs9*, a negative regulator of G-protein signaling, and *Itpr1*, encoding the inositol 1,4,5-trisphosphate receptor type 1, a calcium channel localized to the endoplasmic reticulum. We evaluated the effects of these genes by four metrics: (i) overlap of HetKO-associated DEGs (Table S19) with genes in M43 (Fig. 6A; Table S20); (ii) overlap of HetKO-associated DEGs with the broader set of CIE-associated DEGs (Fig. 6A; Table S20); (iii) Coordinated up- or down-regulation of the M43 eigengene and of its component genes (Fig. 6B, C); and (iv) correlations between the fold change in HetKO vs. wildtype mice compared to the fold change in CIE vs. control mice (Fig. 6D). HetKO for six of the seven hub genes (all but *Zswim6*) was significantly associated with at least one of these metrics. Interestingly, we observed bidirectional effects. HetKO of *Bcl11b, Foxp1, Pde10a*, and *Rarb* mimicked CIE: i.e., genes in M43 were down-regulated and/or we observed positive correlations with the effects of CIE across all CIE-associated DEGs. By contrast, HetKO of *Rgs9* and *Itgr1* had opposite effects: genes in M43 were up-regulated, and we observed negative correlations with effects of CIE across all CIE-associated DEGs. Thus, genetic perturbations unmasked both inhibitory and activating effects of M43 hub genes. Overall, these results validate M43 hub genes as causal regulators for the transcriptional effects of CIE in the striatum.

DISCUSSION

The data presented here provide insight into the cell type-specific effects of chronic intermittent ethanol exposure on gene expression in the dorsal striatum, a key brain region implicated in AUD. The most robust finding was the down-regulation in SPNs of genes involved in postsynaptic signaling cascades. Neuroinflammation-related genes were

also down-regulated. Although we identified very few DEGs in non-neuronal cell types at stringent significance thresholds, the patterns of differential gene expression point to inflammation-related changes in many cell types, as well as potential angiogenic signatures in vascular cells. Finally, hub genes of a gene co-expression module enriched for synaptic signaling genes, M43, were validated as causal regulators of CIE-related transcriptional changes in the striatum.

Multiple results suggested down-regulation of synaptic signaling pathways in SPNs. Notably, our network analysis revealed distinct down-regulated modules, M43 and M29, that were enriched for components of cAMP signaling and BDNF signaling, respectively. cAMP signaling components such as the M43 hub gene *Pde7b* act downstream of postsynaptic dopamine receptors in canonical SPNs. PDE7B is involved in the intricate balance of neuronal growth and pruning that shapes neuronal plasticity and has previously been implicated in neurodegenerative diseases. Studies in neurodegenerative diseases, especially Parkinson's disease, found that PDE7B inhibition attenuated neurodegenerative decline, possibly preventing the loss of dopaminergic neurons [56–58]. Phosphodiesterase inhibitors have been tested on a variety of brain disorders, including AUD [59]. In addition, dopamine signaling through the D1 receptor upregulates *Pde7b*, suggesting a downregulation in D1 receptor signaling in chronic ethanol exposure, which is supported by literature highlighting dysregulation of dopaminergic signaling [60–63].

The BDNF receptor *Ntrk2*/TrkB and other components of receptor tyrosine kinase signaling cascades were also down-regulated in SPNs and were enriched in module M29. *NTRK2* is implicated in AUD [64]. NTRK2 acts as a high-affinity receptor for brain derived neurotrophic factor (BDNF), and also has affinity for neurotrophin-3 and neurotrophin-4. These peptides and signaling cascades are involved in diverse physiological processes including synaptic plasticity, differentiation, and neuronal growth [64–66]. In the striatum, BDNF originating from cortical and substantia nigra neurons binds NTRK2 to initiate several signaling cascades [67, 68]. The *Bdnf* gene itself did not exhibit a clear signal of differential expression in our analysis, despite the important role that dorsal striatal BDNF plays in gating alcohol consumption [69].

Our analysis also shows down-regulation of a neuroinflammatory module, M8. M8 contains ten genes annotated to the cytokine-cytokine signaling pathway, most of which had negative fold-changes in multiple striatal cell types. Several of these genes encode receptors for the pro-inflammatory cytokines IL1, IL12, IL3, IL5, and TNF (*Il1r2*, *Il12rb2*, *Cx3cr1*, *Ccr9*, and *Tnfrsf9*, respectively). M8 also includes genes encoding erythropoietin (*Epo*) and leukemia inhibitory factor receptor (*Lifr*), which have anti-inflammatory functions [70–73]. Likewise, down-regulated genes in M8 annotated to the broader "inflammatory response" pathway included both pro-inflammatory (*Aim2*, *Lrrc12*, and *Ptgis*) [74–76] and anti-inflammatory genes (*Fbxl2, Ptger4 Otulin, Spata2, Gps2)* [77–81]. Thus, chronic ethanol exposure in this mouse model was associated with the suppression of both pro- and anti-inflammatory genes, suggesting a complex change in inflammatory state. Down-regulation of these genes may be surprising, as studies of AUD have consistently found increases in circulating cytokines and markers of neuroinflammation [82–85]. The innate immune response to chronic alcohol, facilitated by TLR receptors, pro-inflammatory cytokines, and signaling between microglia

and other cell types, has been identified as a key element of AUD with the potential for druggable targets [86]. Acute vs. chronic phases of inflammation often involve bidirectional changes in the expression of inflammatory signaling cascades, so one explanation may be that our mouse model captures a different stage of inflammation than that captured in many studies of AUD in humans. Alternatively, the down-regulation of pro-inflammatory receptors in the brain may be a response to an increase in peripheral cytokines and neuroinflammation. There is a need for additional studies to further characterize these inflammatory signatures and their relationship with the changes in neural circuit function.

Despite lower statistical power for rare cell types, our data also suggest altered states of non-neuronal cell types. For instance, our data support angiogenesis-related gene expression changes in endothelial and mural cells. Top DEGs in endothelial cells included *Hes1*, *Tmem252* and *Tgfb2*. *Hes1* is a transcription factor that acts as an effector for the Notch signaling pathway, whose activation inhibits vascular cell differentiation and angiogenesis [87, 88]. Down-regulation of *Notch1* and *Hes1* promote angiogenic cell sprouting and inhibit vascular repair following insult [87, 89, 90]. *Tmem252* is a stalk-cell marker involved in angiogenesis and neovascularization. *Tgfb2* encodes for TGF-B2, which is a dynamic actor that can either inhibit or support angiogenesis [91, 92]. Thus, although there were few DEGs in endothelial cells, many can be interpreted as indicators of increased angiogenesis after CIE. An increase in angiogenesis in response to ethanol exposure may disrupt the blood brain barrier and play a role in the neuroinflammation seen in CIE [54, 83, 93, 94]. Functional studies, especially those centered on the genes identified above and the blood brain barrier, would be of value.

Previous snRNA-seq studies profiled the effects of CIE in the prefrontal cortex of mice and central amygdala from rats [95, 96]. Extended amygdala circuits have important roles in the regulation of negative emotional states and withdrawal, while the prefrontal cortex contributes to cognitive aspects of addiction. All of these studies reported a combination of cell type-specific gene expression changes that can be attributed to forms of neuroplasticity and neuroinflammation. However, the precise genes dysregulated appear to be quite specific to particular neuronal subtypes and phases of addiction. In particular, many of the DEGs we identified in module M43 are expressed specifically in SPNs and their dysregulation is likely specific to this circuit. There is a need for more systematic genomic studies to elucidate the effects of addictive substances across brain regions and contexts.

We identified several genes in module M43 with translational potential. Haploinsufficiency of *Bcl11b*, *Foxp1*, *Pde10a, Rarb*, *Rgs9*, and *Itpr1* each led to gene expression changes that overlapped M43 and/or the broader set of DEGs in CIE-exposed mice. Thus, hub genes of M43 can be targeted to alter the transcriptional states of striatal neurons. The DrugDev database lists 17 genes in M43, including *Pde10a*, as repurposing candidates targeted by approved small molecules and biotherapeutic drugs and clinical-phase drug candidates. An additional 19 genes in M43 encode potentially druggable proteins in druggable gene families (Fig. S18B) [97]. Notably, Logrip and colleagues discovered that injection of TP-10, a PDE10A inhibitor, into the dorsolateral striatum of rats significantly decreased alcohol, but not sucrose, consumption [98]. Given that PDE10A is selectively expressed in striatal SPNs with little appreciable expression elsewhere in the brain, the present data further validate this

gene as a potential target for pharmacotherapy in AUD that may possess relatively low side effect liability [59, 99]. These initial successes in targeting PDE10A for AUD validate the present approach of discovering novel drug targets using snRNA-seq in mouse CIE models and warrants further investigation of the genes we prioritized.

When considering how to leverage the present dataset for therapeutic strategy development, biological context should be carefully considered. For instance, while logic would suggest that a decrease in expression of a gene target should be treated by functional activation of its cognate protein, the opposite is the case for *Pde10a*, which is decreased in expression in response to CIE, while inhibition of PDE10A reduces alcohol consumption [98]. Thus, a gene expression change may reflect a compensatory mechanism that may need to be enhanced for therapeutic benefit. In the case of module M43, down-regulation may be a consequence of decreased synaptic drive onto SPNs. As such, inhibiting an inhibitor of D1 dopamine receptor signaling (e.g., PDE10A) may represent a logical therapeutic approach supported by data [16, 100–102].

We note several limitations of our study and opportunities for future work. Our dataset was better powered to detect differentially expressed genes in common cell types than rare cell types. Thus, the three well-studied interneuron populations of the dorsal striatum -- including the low-threshold spiking somatostatin-expressing INs, the fast-spiking parvalbumin-expressing INs, and the tonically firing cholinergic choline acetyltransferase-expressing INs -- require deeper assessment. Larger samples would be required to detect subtle changes in these cell types. In addition, transcriptional effects of alcohol may vary across striatal sub-regions. These sub-region-specific effects could be elucidated through additional spatial transcriptomics studies, comparing CIE-exposed vs. control animals. Transcriptional effects of alcohol may also vary dynamically across different phases of exposure. It will be valuable to assess these temporal patterns, comparing the CIE paradigm to other models of alcohol exposure, including models with a behavioral (alcohol drinking) component [103]. Sex differences may be under-represented in our dataset due to imprecision in the demultiplexing of cells from male and female mice that were sequenced together. Our discovery and replication datasets utilized distinct pooling strategies and methods for nuclei isolation, potentially making them more difficult to compare. Our findings lay the groundwork for functional studies to test causal roles for differentially expressed genes and gene networks as mediators of alcohol effects on striatal circuits and related behavior. Given the concordant evidence for M43 in our snRNA-seq of mouse CIE and genetic risk for human AUD, single-cell genomic data from the dorsal striatum of humans with AUD is warranted to further validate the translational capacity of the presently identified gene targets.

Supplementary Material

Refer to Web version on PubMed Central for supplementary material.

ACKNOWLEDGEMENTS

This study was supported by grants from the National Institute on Alcohol Abuse and Alcoholism (R01 AA024845, BNM, PI) and the National Institute on Drug Abuse (U01 DA051947, SAA and MKL, PIs). This research is

based in part on data from the Million Veteran Program (MVP), Office of Research and Development, Veterans Health Administration, and was supported by award #I01 BX004820 and the Veterans Integrated Service Network 4 Mental Illness Research, Education and Clinical Center. This publication does not represent the views of the Department of Veteran Affairs or the United States Government.

COMPETING INTERESTS

Dr. Kranzler is a member of advisory boards for Altimmune, Clearmind Medicine, Dicerna Pharmaceuticals, Enthion Pharmaceuticals, and Sophrosyne Pharmaceuticals; a consultant to Sobrera Pharmaceuticals and Altimmune; the recipient of research funding and medication supplies for an investigator-initiated study from Alkermes; a member of the American Society of Clinical Psychopharmacology's Alcohol Clinical Trials Initiative, which was supported in the last three years by Alkermes, Dicerna, Ethypharm, Lundbeck, Mitsubishi, Otsuka, and Pear Therapeutics; and a holder of U.S. patent 10,900,082 titled: "Genotype-guided dosing of opioid agonists," issued 26 January 2021. All other authors declare they have nothing to disclose.

DATA AVAILABILITY

Sequencing data have been uploaded to the Gene Expression Omnibus (GSE292642, GSE292791). All other data are presented in the main text and supplementary figures and tables.

CODE AVAILABILITY

Code used in the data analysis is available at www.github.com/seth-ament/cie-snrnaseq.

REFERENCES

1. Kranzler HR. Overview of alcohol use disorder. Am J Psychiatry. 2023;180:565–72. [PubMed: 37525595]
2. Mason BJ, Heyser CJ. Alcohol use disorder: the role of medication in recovery. Alcohol Res. 2021;41:7.
3. Koob GF, Volkow ND. Neurobiology of addiction: a neurocircuitry analysis. Lancet Psychiatry. 2016;3:760–73. [PubMed: 27475769]
4. Mancini A, Ghiglieri V, Parnetti L, Calabresi P, Di Filippo M. Neuro-immune crosstalk in the striatum: from basal ganglia physiology to circuit dysfunction. Front Immunol. 2021;12:644294. [PubMed: 33953715]
5. Gokce O, Stanley GM, Treutlein B, Neff NF, Camp JG, Malenka RC, et al. Cellular taxonomy of the mouse striatum as revealed by single-cell RNA-seq. Cell Rep. 2016;16:1126–37. [PubMed: 27425622]
6. Saunders A, Macosko EZ, Wysoker A, Goldman M, Krienen FM, de Rivera H, et al. Molecular diversity and specializations among the cells of the adult mouse brain. Cell. 2018;174:1015–30.e16. [PubMed: 30096299]
7. Fieblinger T Striatal control of movement: a role for new neuronal (sub-) populations? Front Hum Neurosci. 2021;15:697284. [PubMed: 34354577]
8. Patton MS, Heckman M, Kim C, Mu C, Mathur BN. Compulsive alcohol consumption is regulated by dorsal striatum fast-spiking interneurons. Neuropsychopharmacology. 2021;46:351–9. [PubMed: 32663841]
9. Egervari G, Siciliano CA, Whiteley EL, Ron D. Alcohol and the brain: from genes to circuits. Trends Neurosci. 2021;44:1004–15. [PubMed: 34702580]
10. Wang J, Lanfranco MF, Gibb SL, Yowell QV, Carnicella S, Ron D. Long-lasting adaptations of the NR2B-containing NMDA receptors in the dorsomedial striatum play a crucial role in alcohol consumption and relapse. J Neurosci. 2010;30:10187–98. [PubMed: 20668202]
11. Wang J, Hamida SB, Darcq E, Zhu W, Gibb SL, Lanfranco MF, et al. Ethanol-mediated facilitation of AMPA receptor function in the dorsomedial striatum: implications for alcohol drinking behavior. J Neurosci. 2012;32:15124–32. [PubMed: 23100433]

12. Ron D, Wang J. The NMDA receptor and alcohol addiction. In: Van Dongen AM, editors. Biology of the NMDA receptor. Boca Raton (FL): CRC Press/Taylor & Francis; 2009.
13. Choi SJ, Kim KJ, Cho HS, Kim SY, Cho YJ, Hahn SJ, et al. Acute inhibition of corticostriatal synaptic transmission in the rat dorsal striatum by ethanol. Alcohol. 2006;40:95–101. [PubMed: 17307645]
14. Haggerty DL, Munoz B, Pennington T, Di Prisco GV, Grecco GG, Atwood BK. The role of anterior insular cortex inputs to dorsolateral striatum in binge alcohol drinking. eLife. 2022;11:e77411. [PubMed: 36098397]
15. Blomeley CP, Cains S, Smith R, Bracci E. Ethanol affects striatal interneurons directly and projection neurons through a reduction in cholinergic tone. Neuropsychopharmacology. 2011;36:1033–46. [PubMed: 21289603]
16. Patton MH, Roberts BM, Lovinger DM, Mathur BN. Ethanol disinhibits dorsolateral striatal medium spiny neurons through activation of a presynaptic delta opioid receptor. Neuropsychopharmacology. 2016;41:1831–40. [PubMed: 26758662]
17. Patton MS, Sheats SH, Siclair AN, Mathur BN. Alcohol potentiates multiple GABAergic inputs to dorsal striatum fast-spiking interneurons. Neuropharmacology. 2023;232:109527. [PubMed: 37011784]
18. Banerjee N Neurotransmitters in alcoholism: a review of neurobiological and genetic studies. Indian J Hum Genet. 2014;20:20–31. [PubMed: 24959010]
19. Miller CN, Kamens HM. The role of nicotinic acetylcholine receptors in alcohol-related behaviors. Brain Res Bull. 2020;163:135–42. [PubMed: 32707263]
20. Tupala E, Tiihonen J. Dopamine and alcoholism: neurobiological basis of ethanol abuse. Prog Neuropsychopharmacol Biol Psychiatry. 2004;28:1221–47. [PubMed: 15588749]
21. Sarkisyan D, Hussain MZ, Watanabe H, Kononenko O, Bazov I, Zhou X, et al. Downregulation of the endogenous opioid peptides in the dorsal striatum of human alcoholics. Front Cell Neurosci. 2015;9:187. [PubMed: 26029055]
22. Adermark L, Jonsson S, Ericson M, Söderpalm B. Intermittent ethanol consumption depresses endocannabinoid-signaling in the dorsolateral striatum of rat. Neuropharmacology. 2011;61:1160–5. [PubMed: 21251919]
23. Jeanblanc J, He D-Y, Carnicella S, Kharazia V, Janak PH, Ron D. Endogenous BDNF in the dorsolateral striatum gates alcohol drinking. J Neurosci. 2009;29:13494–502. [PubMed: 19864562]
24. Mews P, Cunningham AM, Scarpa J, Ramakrishnan A, Hicks EM, Bolnick S, et al. Convergent abnormalities in striatal gene networks in human cocaine use disorder and mouse cocaine administration models. Sci Adv. 2023;9:eadd8946. [PubMed: 36763659]
25. Phan BN, Ray MH, Xue X, Fu C, Fenster RJ, Kohut SJ, et al. Single nuclei transcriptomics in human and non-human primate striatum in opioid use disorder. Nat Commun. 2024;15:878. [PubMed: 38296993]
26. Sinirlioglu ZA, Coskunpinar E, Akbas F. miRNA and mRNA expression profiling in rat brain following alcohol dependence and withdrawal. Cell Mol Biol. 2017;63:49–56.
27. Darlington TM, McCarthy RD, Cox RJ, Miyamoto-Ditmon J, Gallego X, Ehringer MA. Voluntary wheel running reduces voluntary consumption of ethanol in mice: identification of candidate genes through striatal gene expression profiling. Genes Brain Behav. 2016;15:474–90. [PubMed: 27063791]
28. Piechota M, Korostynski M, Solecki W, Gieryk A, Slezak M, Bilecki W, et al. The dissection of transcriptional modules regulated by various drugs of abuse in the mouse striatum. Genome Biol. 2010;11:R48. [PubMed: 20459597]
29. Brenner E, Tiwari GR, Kapoor M, Liu Y, Brock A, Mayfield RD. Single cell transcriptome profiling of the human alcohol-dependent brain. Hum Mol Genet. 2020;29:1144–53. [PubMed: 32142123]
30. Erickson EK, Farris SP, Blednov YA, Mayfield RD, Harris RA. Astrocyte-specific transcriptome responses to chronic ethanol consumption. Pharmacogenomics J. 2018;18:578–89. [PubMed: 29305589]

31. McCarthy GM, Farris SP, Blednov YA, Harris RA, Mayfield RD. Microglial-specific transcriptome changes following chronic alcohol consumption. Neuropharmacology. 2018;128:416–24. [PubMed: 29101021]
32. van den Oord EJ, Xie LY, Zhao M, Aberg KA, Clark SL. A single-nucleus transcriptomics study of alcohol use disorder in the nucleus accumbens. Addict Biol. 2023;28:e13250. [PubMed: 36577731]
33. Becker HC, Lopez MF. Increased ethanol drinking after repeated chronic ethanol exposure and withdrawal experience in C57BL/6 mice. Alcohol Clin Exp Res. 2004;28:1829–38. [PubMed: 15608599]
34. Malaiya S, Cortes-Gutierrez M, Herb BR, Coffey SR, Legg SRW, Cantle JP, et al. Single-nucleus RNA-seq reveals dysregulation of striatal cell identity due to Huntington's disease mutations. J Neurosci. 2021;41:5534–52. [PubMed: 34011527]
35. Kamath T, Abdulraouf A, Burris SJ, Langlieb J, Gazestani V, Nadaf NM, et al. Single-cell genomic profiling of human dopamine neurons identifies a population that selectively degenerates in Parkinson's disease. Nat Neurosci. 2022;25:588–95. [PubMed: 35513515]
36. Germain P-L, Lun A, Garcia Meixide C, Macnair W, Robinson MD. Doublet identification in single-cell sequencing data using scDblFinder. F1000Res. 2022;10:979.
37. Hao Y, Hao S, Andersen-Nissen E, Mauck WM, Zheng S, Butler A, et al. Integrated analysis of multimodal single-cell data. Cell. 2021;184:3573–87.e29. [PubMed: 34062119]
38. Korsunsky I, Millard N, Fan J, Slowikowski K, Zhang F, Wei K, et al. Fast, sensitive and accurate integration of single-cell data with harmony. Nat Methods. 2019;16:1289–96. [PubMed: 31740819]
39. Linderman GC, Zhao J, Roulis M, Bielecki P, Flavell RA, Nadler B, et al. Zero-preserving imputation of single-cell RNA-seq data. Nat Commun. 2022;13:192. [PubMed: 35017482]
40. Robinson MD, McCarthy DJ, Smyth GK. edgeR: a Bioconductor package for differential expression analysis of digital gene expression data. Bioinformatics. 2010;26:139–40. [PubMed: 19910308]
41. Murphy AE, Skene NG. A balanced measure shows superior performance of pseudobulk methods in single-cell RNA-sequencing analysis. Nat Commun. 2022;13:7851. [PubMed: 36550119]
42. Zhang Y, Parmigiani G, Johnson WE. ComBat-seq: batch effect adjustment for RNA-seq count data. NAR Genom Bioinform. 2020;2:lqaa078. [PubMed: 33015620]
43. Ritchie ME, Phipson B, Wu D, Hu Y, Law CW, Shi W, et al. limma powers differential expression analyses for RNA-sequencing and microarray studies. Nucleic Acids Res. 2015;43:e47. [PubMed: 25605792]
44. Ament SA, Cortes-Gutierrez M, Herb BR, Mocci E, Colantuoni C, McCarthy MM. A single-cell genomic atlas for maturation of the human cerebellum during early childhood. Sci Transl Med. 2023;15:eade1283. [PubMed: 37824600]
45. Kember RL, Vickers-Smith R, Zhou H, Xu H, Jennings M, Dao C, et al. Genetic underpinnings of the transition from alcohol consumption to alcohol use disorder: shared and unique genetic architectures in a cross-ancestry sample. Am J Psychiatry. 2023;180:584–93. [PubMed: 37282553]
46. de Leeuw CA, Mooij JM, Heskes T, Posthuma D. MAGMA: generalized gene-set analysis of GWAS data. PLoS Comput Biol. 2015;11:e1004219. [PubMed: 25885710]
47. Wang N, Langfelder P, Stricos M, Ramanathan L, Richman JB, Vaca R, et al. Mapping brain gene coexpression in daytime transcriptomes unveils diurnal molecular networks and deciphers perturbation gene signatures. Neuron. 2022;110:3318–38.e9. [PubMed: 36265442]
48. Law CW, Chen Y, Shi W, Smyth GK. voom: Precision weights unlock linear model analysis tools for RNA-seq read counts. Genome Biol. 2014;15:R29. [PubMed: 24485249]
49. Lopez MF, Becker HC. Effect of pattern and number of chronic ethanol exposures on subsequent voluntary ethanol intake in C57BL/6J mice. Psychopharmacology. 2005;181:688–96. [PubMed: 16001125]
50. Griffin WC, Lopez MF, Becker HC. Intensity and duration of chronic ethanol exposure is critical for subsequent escalation of voluntary ethanol drinking in mice. Alcohol Clin Exp Res. 2009;33:1893–900. [PubMed: 19673744]

51. Plaisier SB, Taschereau R, Wong JA, Graeber TG. Rank–rank hypergeometric overlap: identification of statistically significant overlap between gene-expression signatures. Nucleic Acids Res. 2010;38:e169. [PubMed: 20660011]
52. Li J, Li C, Loreno EG, Miriyala S, Panchatcharam M, Lu X, et al. Chronic low-dose alcohol consumption promotes cerebral angiogenesis in mice. Front Cardiovasc Med. 2021;8:681627. [PubMed: 34869620]
53. Morrow D, Cullen JP, Cahill PA, Redmond EM. Ethanol stimulates endothelial cell angiogenic activity via a Notch- and angiopoietin-1-dependent pathway. Cardiovasc Res. 2008;79:313–21. [PubMed: 18448572]
54. Nakayama K, Hasegawa H. Blood vessels as a key mediator for ethanol toxicity: implication for neuronal damage. Life. 2022;12:1882. [PubMed: 36431016]
55. Gaziano JM, Concato J, Brophy M, Fiore L, Pyarajan S, Breeling J, et al. Million veteran program: a mega-biobank to study genetic influences on health and disease. J Clin Epidemiol. 2016;70:214–23. [PubMed: 26441289]
56. Morales-Garcia JA, Redondo M, Alonso-Gil S, Gil C, Perez C, Martinez A, et al. Phosphodiesterase 7 inhibition preserves dopaminergic neurons in cellular and rodent models of parkinson disease. PLoS ONE. 2011;6:e17240. [PubMed: 21390306]
57. Morales-Garcia JA, Aguilar-Morante D, Hernandez-Encinas E, Alonso-Gil S, Gil C, Martinez A, et al. Silencing phosphodiesterase 7B gene by lentiviral-shRNA interference attenuates neurodegeneration and motor deficits in hemi-parkinsonian mice. Neurobiol Aging. 2015;36:1160–73. [PubMed: 25457552]
58. Erro R, Mencacci NE, Bhatia KP. The emerging role of phosphodiesterases in movement disorders. Mov Disord. 2021;36:2225–43. [PubMed: 34155691]
59. Logrip ML. Phosphodiesterase regulation of alcohol drinking in rodents. Alcohol. 2015;49:795–802. [PubMed: 26095589]
60. Salinas AG, Mateo Y, Cuzon Carlson VC, Stinnett GS, Luo G, Seasholtz AF, et al. Long-term alcohol consumption alters dorsal striatal dopamine release and regulation by D2 dopamine receptors in rhesus macaques. Neuropsychopharmacology. 2021;46:1432–41. [PubMed: 33452430]
61. Trantham-Davidson H, Chandler LJ. Alcohol-induced alterations in dopamine modulation of prefrontal activity. Alcohol. 2015;49:773–9. [PubMed: 26558348]
62. Heinz A, Siessmeier T, Wrase J, Hermann D, Klein S, Grüsser SM, et al. Correlation between dopamine D2 receptors in the ventral striatum and central processing of alcohol cues and craving. Am J Psychiatry. 2004;161:1783–9. [PubMed: 15465974]
63. Feltmann K, Borroto-Escuela DO, Rüegg J, Pinton L, de Oliveira Sergio T, Narváez M, et al. Effects of long-term alcohol drinking on the dopamine D2 receptor: gene expression and heteroreceptor complexes in the striatum in rats. Alcohol Clin Exp Res. 2018;42:338–51. [PubMed: 29205397]
64. Hamada K, Lasek AW. Receptor tyrosine kinases as therapeutic targets for alcohol use disorder. Neurotherapeutics. 2020;17:4–16. [PubMed: 31617071]
65. Deinhardt K, Chao MV. Trk receptors. In: Lewin GR & Carter BD, editors. Neurotrophic factors. Berlin, Heidelberg: Springer; 2014. pp. 103–19.
66. Gupta VK, You Y, Gupta VB, Klistorner A, Graham SL. TrkB receptor signalling: implications in neurodegenerative, psychiatric and proliferative disorders. Int J Mol Sci. 2013;14:10122–42. [PubMed: 23670594]
67. Altar CA, Cai N, Bliven T, Juhasz M, Conner JM, Acheson AL, et al. Anterograde transport of brain-derived neurotrophic factor and its role in the brain. Nature. 1997;389:856–60. [PubMed: 9349818]
68. Li Y, Yui D, Luikart BW, McKay RM, Li Y, Rubenstein JL, et al. Conditional ablation of brain-derived neurotrophic factor-TrkB signaling impairs striatal neuron development. Proc Natl Acad Sci. 2012;109:15491–6. [PubMed: 22949667]
69. Logrip ML, Barak S, Warnault V, Ron D. Corticostriatal BDNF and alcohol addiction. Brain Res. 2015;1628:60–67. [PubMed: 25801118]

70. Ghezzi P, Bigini P, Mengozzi M Role of Erythropoietin in Inflammatory Pathologies of the CNS. In: Höke A, editors. Erythropoietin and the nervous system: novel therapeutic options for neuroprotection. Boston, MA: Springer US; 2006. pp. 191–209
71. Rey F, Balsari A, Giallongo T, Ottolenghi S, Di Giulio AM, Samaja M, et al. Erythropoietin as a neuroprotective molecule: an overview of its therapeutic potential in neurodegenerative diseases. ASN Neuro. 2019;11:1759091419871420.
72. Hendriks JJA, Slaets H, Carmans S, de Vries HE, Dijkstra CD, Stinissenet P, et al. Leukemia inhibitory factor modulates production of inflammatory mediators and myelin phagocytosis by macrophages. J Neuroimmunol. 2008;204:52–57. [PubMed: 18771807]
73. Luo Y, Ali T, Liu Z, Gao R, Li A, Yang C, et al. EPO prevents neuroinflammation and relieves depression via JAK/STAT signaling. Life Sci. 2023;333:122102. [PubMed: 37769806]
74. Kim H, Seo JS, Lee S-Y, Ha K-T, Choi BT, Shin Y-I, et al. AIM2 inflammasome contributes to brain injury and chronic post-stroke cognitive impairment in mice. Brain Behav Immun. 2020;87:765–76. [PubMed: 32201254]
75. Chai L, Dai L, Che Y, Xu J, Liu G, Zhang Z, et al. LRRC19, a novel member of the leucine-rich repeat protein family, activates NF-κB and induces expression of proinflammatory cytokines. Biochem Biophys Res Commun. 2009;388:543–8. [PubMed: 19679103]
76. Lima IV, Bastos LF, Limborço-Filho M, Fiebich BL, de Oliveira AC. Role of prostaglandins in neuroinflammatory and neurodegenerative diseases. Mediators Inflamm. 2012;2012:946813. [PubMed: 22778499]
77. Bordon Y Fine-tuning of inflammation by F-box proteins. Nat Rev Immunol. 2013;13:305–305.
78. Na YR, Jung D, Stakenborg M, Jang H, Gu GJ, Jeong MR, et al. Prostaglandin E2 receptor PTGER4-expressing macrophages promote intestinal epithelial barrier regeneration upon inflammation. Gut. 2021;70:2249–60. [PubMed: 33558271]
79. Heger K, Wickliffe KE, Ndoja A, Zhang J, Murthy A, Dugger DL, et al. OTULIN limits cell death and inflammation by deubiquitinating LUBAC. Nature. 2018;559:120–4. [PubMed: 29950720]
80. Ren Y, Jiang J, Jiang W, Zhou X, Lu W, Wang J, et al. Spata2 knockdown exacerbates brain inflammation via NF-κB/P38MAPK signaling and NLRP3 inflammasome activation in cerebral ischemia/reperfusion rats. Neurochem Res. 2021;46:2262–75. [PubMed: 34075523]
81. Cardamone MD, Krones A, Tanasa B, Taylor H, Ricci L, Ohgi KA, et al. A protective strategy against hyperinflammatory responses requiring the nontranscriptional actions of GPS2. Mol Cell. 2012;46:91–104. [PubMed: 22424771]
82. Achur RN, Freeman WM, Vrana KE. Circulating cytokines as biomarkers of alcohol abuse and alcoholism. J Neuroimmune Pharmacol. 2010;5:83–91. [PubMed: 20020329]
83. Adams C, Perry N, Conigrave J, Hurzeler T, Stevens J, Dunbar KPY, et al. Central markers of neuroinflammation in alcohol use disorder: a meta-analysis of neuroimaging, cerebral spinal fluid, and postmortem studies. Alcohol Clin Exp Res. 2023;47:197–208.
84. Erickson EK, Grantham EK, Warden AS, Harris RA. Neuroimmune signaling in alcohol use disorder. Pharmacol Biochem Behav. 2019;177:34–60. [PubMed: 30590091]
85. Lékó AH, Ray LA, Leggio L. The vicious cycle between (neuro)inflammation and alcohol use disorder: an opportunity to develop new medications? Alcohol Clin Exp Res. 2023;47:843–7.
86. Crews FT, Lawrimore CJ, Walter TJ, Coleman LG. The role of neuroimmune signaling in alcoholism. Neuropharmacology. 2017;122:56–73. [PubMed: 28159648]
87. Kitagawa M, Hojo M, Imayoshi I, Goto M, Ando M, Ohtsuka T, et al. Hes1 and Hes5 regulate vascular remodeling and arterial specification of endothelial cells in brain vascular development. Mech Dev. 2013;130:458–66. [PubMed: 23871867]
88. Ohtsuka T, Ishibashi M, Gradwohl G, Nakanishi S, Guillemot F, Kageyama R. Hes1 and Hes5 as Notch effectors in mammalian neuronal differentiation. EMBO J. 1999;18:2196–207. [PubMed: 10205173]
89. Liu Z-J, Xiao M, Balint K, Soma A, Pinnix CC, Capobianco AJ, et al. Inhibition of endothelial cell proliferation by Notch1 signaling is mediated by repressing MAPK and PI3K/Akt pathways and requires MAML1. FASEB J. 2006;20:1009–11. [PubMed: 16571776]

90. Quillard T, Coupel S, Coulon F, Fitau J, Chatelais M, Cuturi MC, et al. Impaired Notch4 activity elicits endothelial cell activation and apoptosis. Arterioscler Thromb Vasc Biol. 2008;28:2258–65. [PubMed: 18802018]

91. Lebrin F, Deckers M, Bertolino P, ten Dijke P. TGF-β receptor function in the endothelium. Cardiovasc Res. 2005;65:599–608. [PubMed: 15664386]

92. Jarad M, Kuczynski EA, Morrison J, Viloria-Petit AM, Coomber BL. Release of endothelial cell associated VEGFR2 during TGF-β modulated angiogenesis in vitro. BMC Cell Biol. 2017;18:10. [PubMed: 28114883]

93. Vore AS, Deak T. Alcohol, inflammation, and blood-brain barrier function in health and disease across development. Int Rev Neurobiol. 2022;161:209–49. [PubMed: 34801170]

94. Carrino D, Branca JJV, Becatti M, Paternostro F, Morucci G, Gulisano M, et al. Alcohol-induced blood-brain barrier impairment: an in vitro study. Int J Environ Res Public Health. 2021;18:2683. [PubMed: 33799986]

95. Dilly GA, Kittleman CW, Kerr TM, Messing RO, Mayfield RD. Cell-type specific changes in PKC-delta neurons of the central amygdala during alcohol withdrawal. Transl Psychiatry. 2022;12:289. [PubMed: 35859068]

96. Salem NA, Manzano L, Keist MW, Ponomareva O, Roberts AJ, Roberto M, et al. Cell-type brain-region specific changes in prefrontal cortex of a mouse model of alcohol dependence. Neurobiol Dis. 2024;190:106361. [PubMed: 37992784]

97. Finan C, Gaulton A, Kruger FA, Lumbers RT, Shah T, Engmann J, et al. The druggable genome and support for target identification and validation in drug development. Sci Transl Med. 2017;9:eaag1166. [PubMed: 28356508]

98. Logrip ML, Vendruscolo LF, Schlosburg JE, Koob GF, Zorrilla EP. Phosphodiesterase 10A regulates alcohol and saccharin self-administration in rats. Neuropsychopharmacology. 2014;39:1722–31. [PubMed: 24549104]

99. Menniti FS, Chappie TA, Schmidt CJ. PDE10A inhibitors-clinical failure or window into antipsychotic drug action? Front Neurosci. 2020;14:600178. [PubMed: 33551724]

100. Cuzon Carlson VC, Seabold GK, Helms CM, Garg N, Odagiri M, Rau AR, et al. Synaptic and morphological neuroadaptations in the putamen associated with long-term, relapsing alcohol drinking in primates. Neuropsychopharmacology. 2011;36:2513–28. [PubMed: 21796110]

101. Wilcox MV, Cuzon Carlson VC, Sherazee N, Sprow GM, Bock R, Thiele TE, et al. Repeated binge-like ethanol drinking alters ethanol drinking patterns and depresses striatal GABAergic transmission. Neuropsychopharmacology. 2014;39:579–94. [PubMed: 23995582]

102. Cuzon Carlson VC, Grant KA, Lovinger DM. Synaptic adaptations to chronic ethanol intake in male rhesus monkey dorsal striatum depend on age of drinking onset. Neuropharmacology. 2018;131:128–42. [PubMed: 29241653]

103. Becker HC & Lopez MF Animal models of excessive alcohol consumption in rodents. Curr Top Behav Neurosci. 2024;1–32 10.1007/7854_2024_461. [PubMed: 37922101]

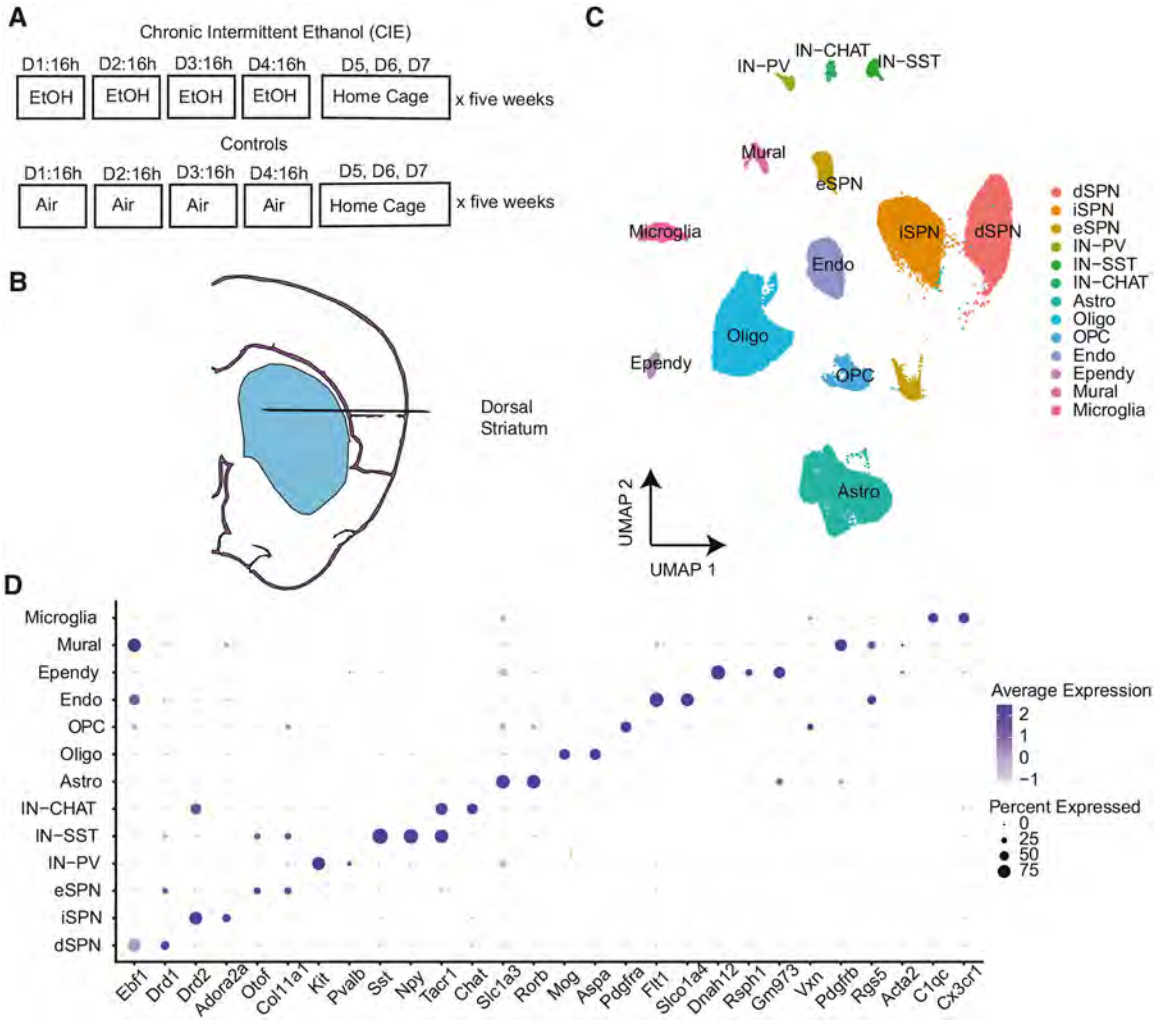

Fig. 1. Single-nuclei RNA sequencing of the mouse dorsal striatum in the context of chronic intermittent ethanol exposure.

A The chronic intermittent ethanol (CIE) paradigm. **B** Location of the dorsal striatum on a coronal section of the mouse brain (reproduced from the Allen Reference Atlas). **C** Uniform manifold approximation and projection (UMAP) plot displaying snRNA-seq cell clusters from the discovery dataset. **D** Dot plot for the expression of cell type marker genes in the discovery dataset. D1-D7, days 1–7; SPN, spiny projection neurons; IN interneurons, Astro astrocytes, Oligo oligodendrocytes, OPC oligodendrocyte precursor cells, Endo endothelial cells, Ependy ependymal cells.

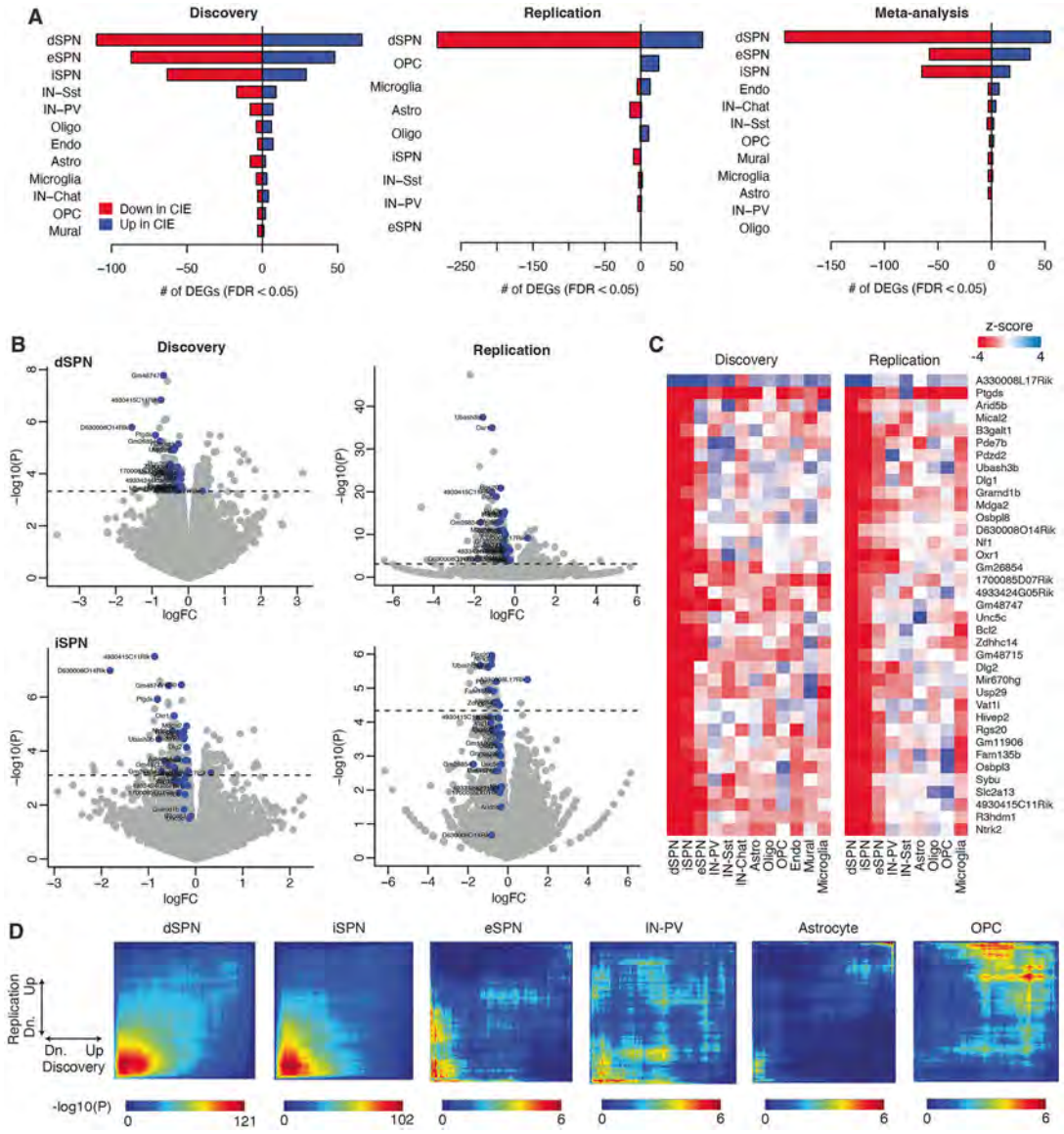

Fig. 2. Discovery and replication of differentially expressed genes in dorsal striatum cell types from chronic intermittent ethanol (CIE)-exposed vs. control mice.

A Counts of cell type-specific up- and down-regulated differentially expressed genes (DEGs; False Discovery Rate [FDR] < 0.05) in the discovery samples, replication sample, and meta-analysis. **B** Volcano plots showing the log2(fold change) and −log10(p-value) for differential gene expression in dSPNs and iSPNs in the discovery and replication samples. Dashed line corresponds to FDR < 0.05. 37 highly-reproducible DEGs with FDR < 0.05 in both samples (primarily in dSPNs) are labeled and highlighted in blue. **C** Effect sizes for the 37 highly-reproducible DEGs across cell types in the discovery and replication samples. **D** Rank-rank hypergeometric overlap plots visualizing the reproducibility of differential expression ranks within six cell types for which the reproducibility was greater than expected by chance (FDR < 0.05). Heatmap color indicates the hypergeometric $-\log_{10}$(p-value) for the overlap between the differential expression gene ranks at multiple thresholds within the discovery and replication datasets. Significant p-values in the lower-left quadrant of each plot indicate

reproducible down-regulation in CIE-exposed vs. control mice, while significant p-values in the upper-right quadrant indicate reproducible up-regulation.

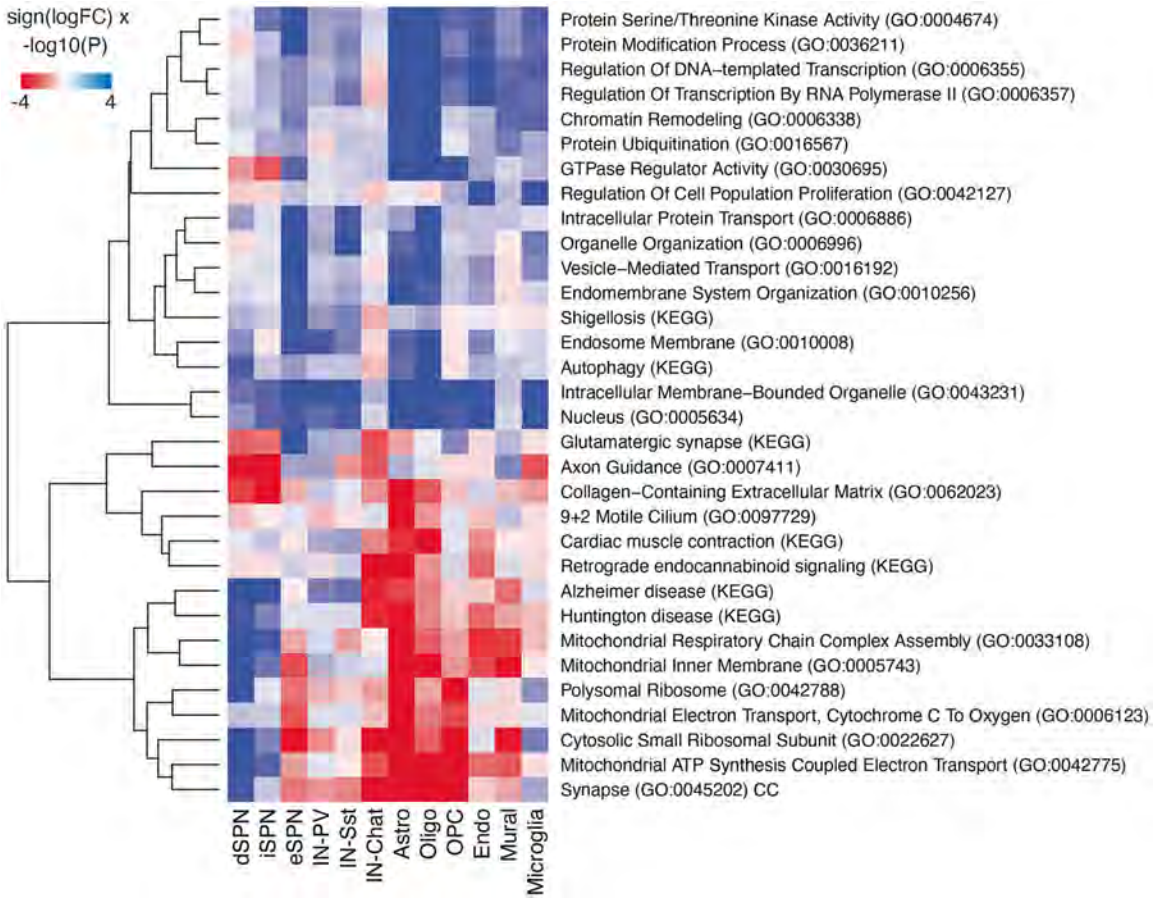

Fig. 3. Gene sets enriched for differential gene expression in CIE vs. control mice.

A total of 217 Gene Ontology and KEGG gene sets were enriched among the differentially expressed genes, significant in at least one cell type at FDR < 0.05. The top 30 gene sets are shown after dropping redundant sets that had substantial overlap with a more-significant set (Cohen's kappa >0.5). $-\log_{10}$(p-values) >4 are indicated by saturated heatmap colors.

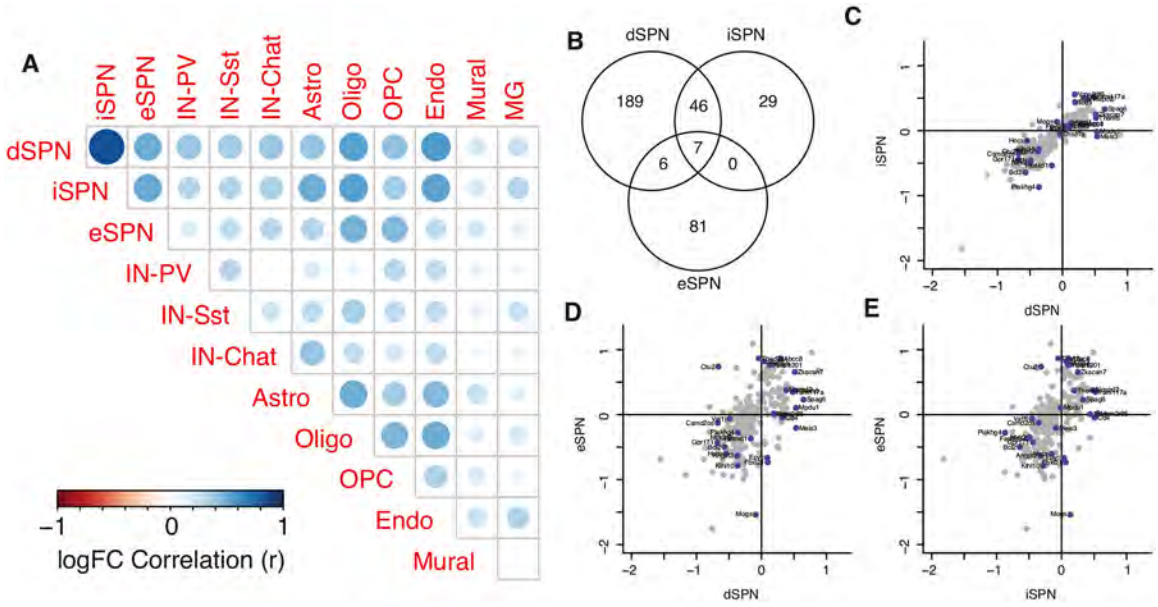

Fig. 4. Cell type-specific vs. shared effects of chronic intermittent ethanol across striatal cell types.

A Heatmap indicating the strengths of correlations between cell types based on the $\log_2$ fold changes of differentially expressed genes in chronic intermittent ethanol-exposed mice vs. controls. **B** Venn diagram indicating the counts of shared vs. unique DEGs in dSPNs, iSPNs, and eSPNs. **C**–**E** Biplots comparing the log2 fold changes of DEGs in dSPNs vs. iSPNs **C**, dSPNs vs. eSPNs **D**, and iSPNs vs. eSPNs **E**. The top five up- and down-regulated DEGs in each cell type are labeled and highlighted in blue.

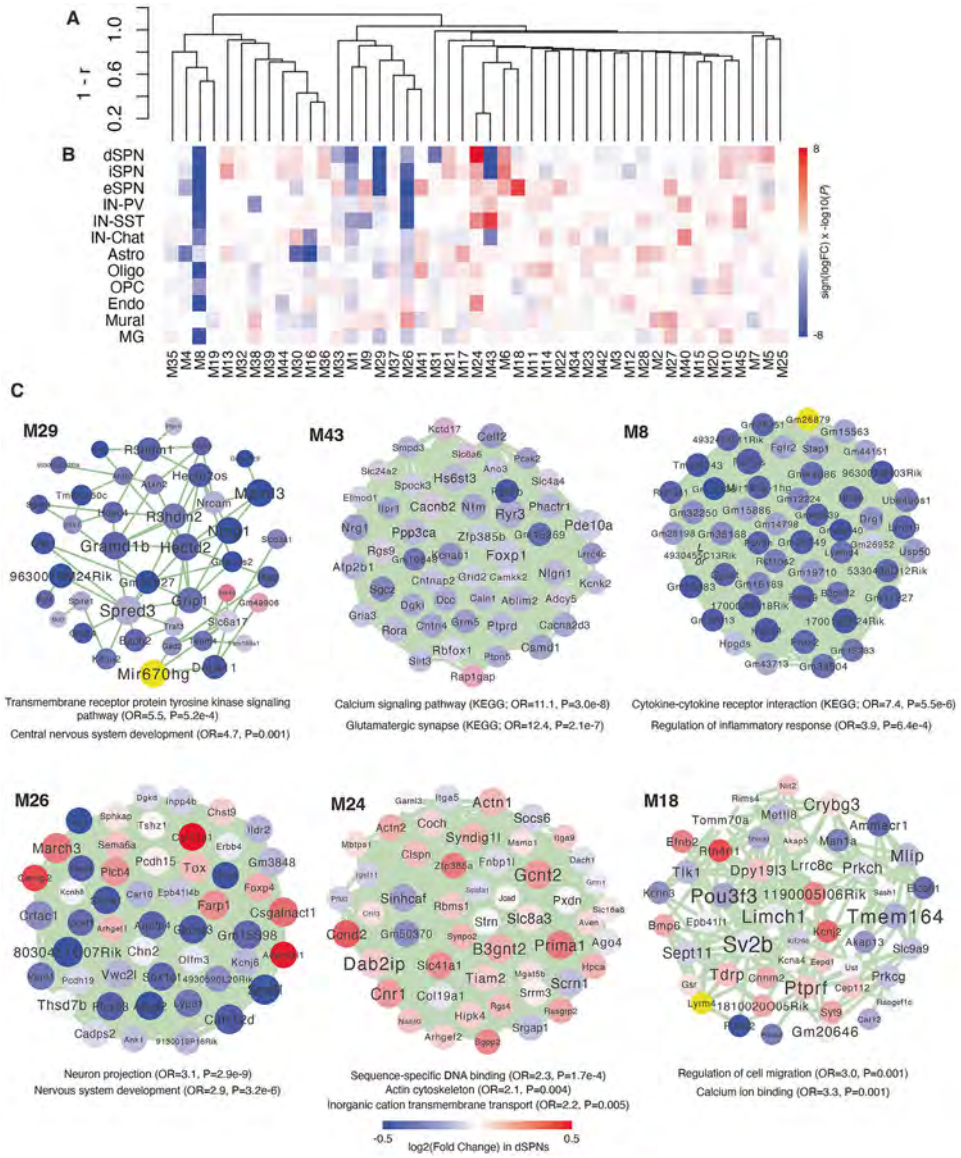

Fig. 5. Gene co-expression networks dysregulated in spiny projection neurons after chronic intermittent ethanol.

A Hierarchical clustering of modules, based on the correlations of their centroids in spiny projection neurons. **B** Enrichments of modules for differentially expressed genes in CIE vs. control mice. Blue and red shades correspond to enrichment for down- and up-regulated DEGs, respectively. **C** The top 50 hub genes in each of six dysregulated modules. Node size corresponds to network centrality. Blue and red shades correspond to negative and positive fold changes in dSPNs from CIE vs. control animals, respectively. Gray lines connecting nodes indicate pairwise gene-gene correlations with Pearson's r > 0.5. We display 2–3 top Gene Ontology and KEGG gene sets over-represented in each module.

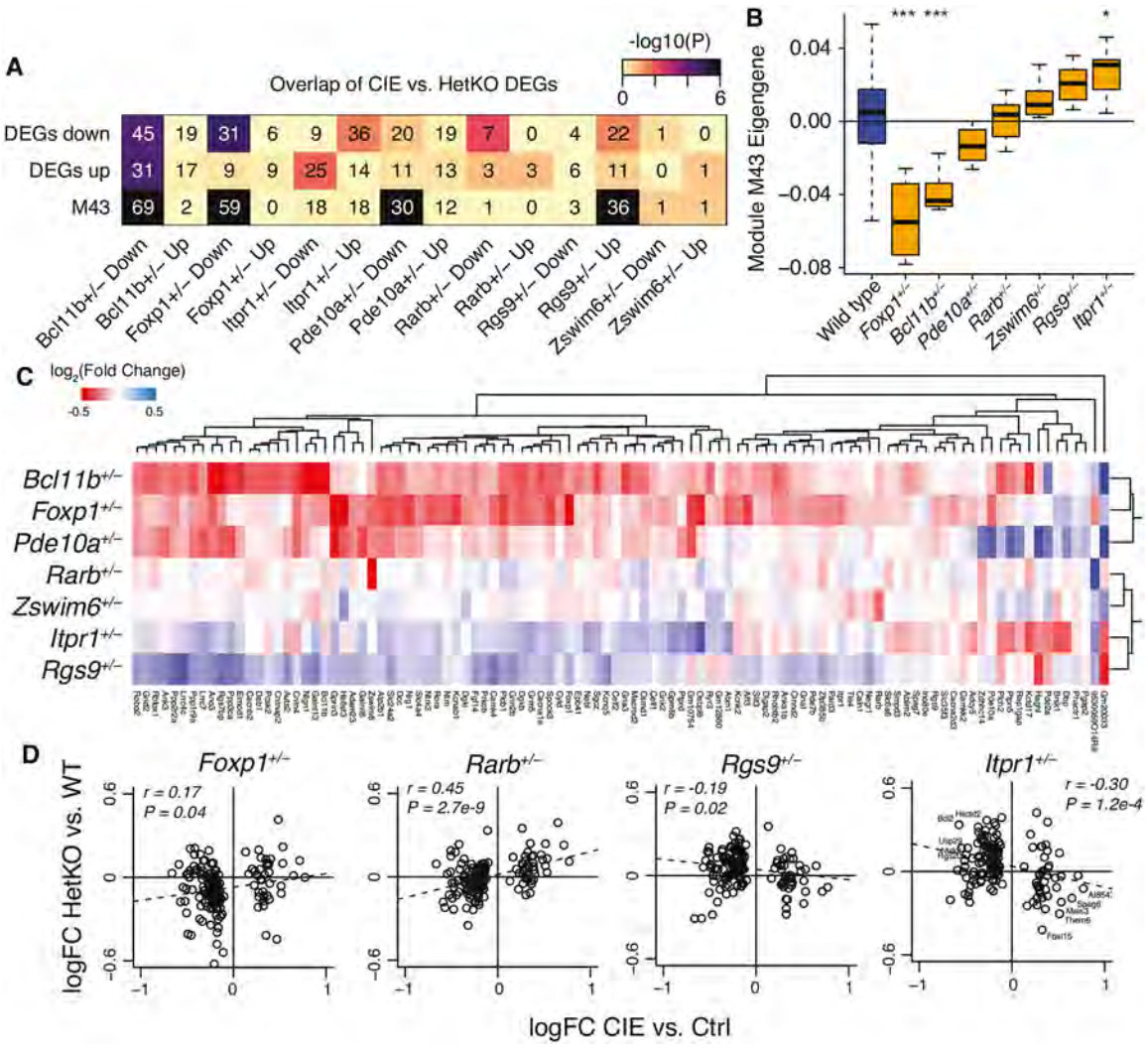

Fig. 6. Causal effects of module M43 hub genes on striatal gene expression.

Effects of seven module M43 hub genes on striatal gene expression were examined using publicly available mRNA-seq from heterozygous knockout (HetKO) mice. We evaluated overlap with the effects of CIE by four metrics. **A** Over-representation of differentially expressed genes (DEGs) in HetKO mice with DEGs in CIE-exposed mice and with genes in module M43. **B** Differential expression of the module M43 eigengene in HetKO mice vs. wildtype controls. $*P < 0.05$; $***P < 0.001$. **C** Heatmap showing the log2(fold changes) of each gene in module M43 in HetKO vs. control mice. **D** Scatter plots showing the $\log_2$(fold changes) of all DEGs in CIE-exposed mice their fold changes in dSPNs of CIE-exposed mice to their fold changes in HetKO mice.